JOURNAL OF MATERIALS SCIENCE **37** (2002) 4235–4245

Dimensional changes and creep of silica core ceramics used in investment casting of superalloys

A. A. WERESZCZAK*, K. BREDER†, M. K. FERBER, T. P. KIRKLAND, E. A. PAYZANT, C. J. RAWN
High Temperature Materials Laboratory, Oak Ridge National Laboratory, Oak Ridge, TN 37831-6069, USA
E-mail: awereszczak@arl.army.mil

E. KRUG, C. L. LAROCCO, R. A. PIETRAS
Carpenter Engineered Molded Ceramic Products, Certech Incorporated, Wood-Ridge, NJ 07075, USA

M. KARAKUS
Department of Ceramic Engineering, University of Missouri-Rolla, Rolla, MO 65409, USA

Dimensional changes and creep deformation of a silica/zircon (74%/24%, respectively) and a high silica (93% silica and 3% zircon) ceramic were characterized and compared. All specimens were tested with a thermal profile that consisted of a 300°C/h heating rate to 1475 or 1525°C, followed by a one-hour isothermal hold (where each specimen was compressively crept under a static stress of 2.07, 4.14, or 6.21 MPa). The specimens were cooled at a rate of 900°C/h under stress. Dimensional changes were interpreted from apparent thermal expansion behavior during heating as well as before-and-after dimensional measurements. The silica/zircon ceramic generally exhibited less total contraction than the high silica ceramic for a specific test condition even though it crept faster at all stresses and temperatures during the one-hour isothermal/isostress segment. This indicates that the total contraction for both was dominated by reinitiated sintering and subsequent cristobalite formation that occurred during the heating segment. Minimum creep rate during the one-hour isothermal/isostress segment was examined as a function of stress and temperature for both ceramics using a power-law creep model. Creep-rate stress exponents (n) and activation energies (Q) were equivalent (within 95% confidence) for both ceramics showing that their different contents of zircon (3 vs. 24%) did not affect them. Lastly, $n \approx 1.3$–1.4 and $Q \approx 170$ kJ/mol indicate that diffusion-assisted crystallization of cristobalite, combined with power-law sintering owing to the high concentration of porosity (28–30%) was likely the rate-limiting mechanism in the creep deformation for both ceramics.

1. Introduction

Fused (vitreous) silica-based ceramics are often used as sacrificial cores in investment metal castings to produce hollow, precise, and complex-shaped structures within them. Their usage is prevalent in the manufacture of superalloy gas turbine components (see Fig. 1) where internal structures, such as cooling passages, are desired. A practical method for forming these internal structures is to cast the metal around a leachable, via chemical means, fused silica ceramic core that has been previously fabricated by injection molding, transfer molding, or rapid prototype printing [1]. Such a casting process often places the following restrictions on the ceramic [2]:

- it must be chemically compatible with the metal;
- it must be much weaker than the metal so that it will crush (i.e., exhibit good "crushability") during metal solidification rather than impose deleterious and destructive high stresses (e.g., those that lead to secondary crystallization in single crystal castings, grain boundary cracking in directionally solidified castings, or hot-tearing in equiaxed castings) into the metal;

Present Address: U. S. Army Research Laboratory, Aberdeen Proving Ground, MD, USA.
†*Present Address:* Saint-Gobain Abrasives, Higgins Grinding Technology Center, Worcester, MA, USA.

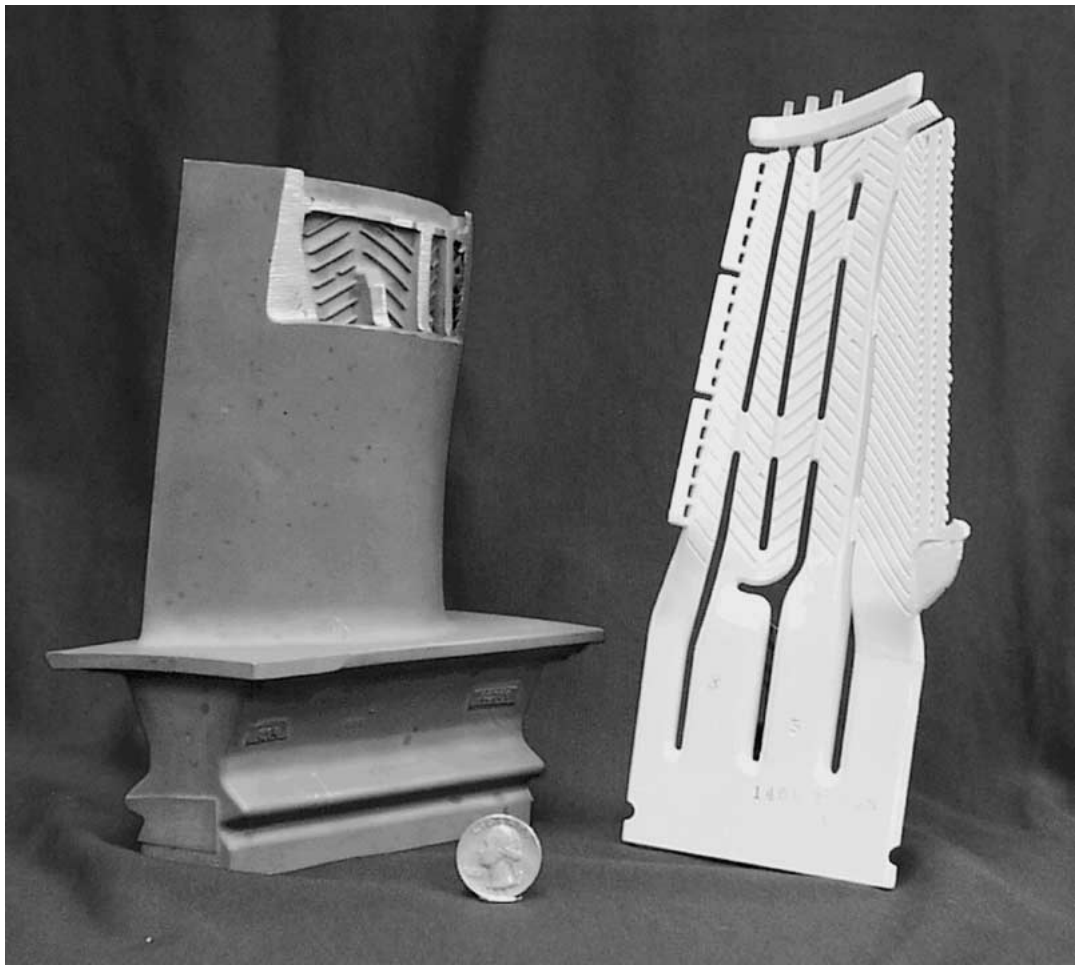

Figure 1 Ceramic core (right) and a sectioned superalloy component (left). The latter shows the intricate interior design that such cores can produce.

- it must have enough strength to be resistant to thermal shock;
- it must be sufficiently resistant to dimensional changes (i.e., exhibit good "stability") and yield a suitable metal surface finish; and
- it must be removable by a process that is not harmful to the metal casting.

A successfully used ceramic core is one in which an optimum compromise between crushability and stability was promoted; namely, the ceramic deformed rapidly enough to allow sufficient stress relaxation in the metal (so that deleteriously high stresses do not initiate defects) and concomitantly being sufficiently rigid or stable so to maintain intended dimensional tolerances of the metal component. Though creep performance of the ceramic affects both the crushability and stability of the core, the primary intent of the present study was to characterize high temperature deformation of the ceramic so to better understand the former.

Because fused silica crystallizes in a temperature regime that the metals are typically cast, and because there is a density difference between its amorphous and crystalline phases, many studies have been performed to examine those thermomechanical effects on the silica's mechanical integrity. Huseby *et al.*, [3] performed a series of quench tests to examine the contraction phenomenon during dilatometry heating, and concluded that observed shrinkage was due to densification by viscous flow sintering of the vitreous silica as well as its devitrification. Others have attempted to model the crystallization process and examine the effects of additives on its control [4–6].

Although fused silica crystallization effects that occur during heating to casting temperatures are numerous in the literature, published data on the silica's creep performance during the isothermal casting process is largely nonexistent though crushability and stability are two of the key criteria listed above. Furthermore, the effects of heating on the non-equilibrium state of the fused silica cannot be discounted either as they can dictate the nature of the existing material state when a creep test is ultimately performed. Consequently, the creep resistances of silica cores were examined while also characterizing the total dimensional changes that result from a representative thermal profile used in metal casting.

The responses of two ceramic cores were examined; one material was a high-zircon-containing fused silica ceramic used in the manufacturing of directionally-solidified or single crystal superalloy components that

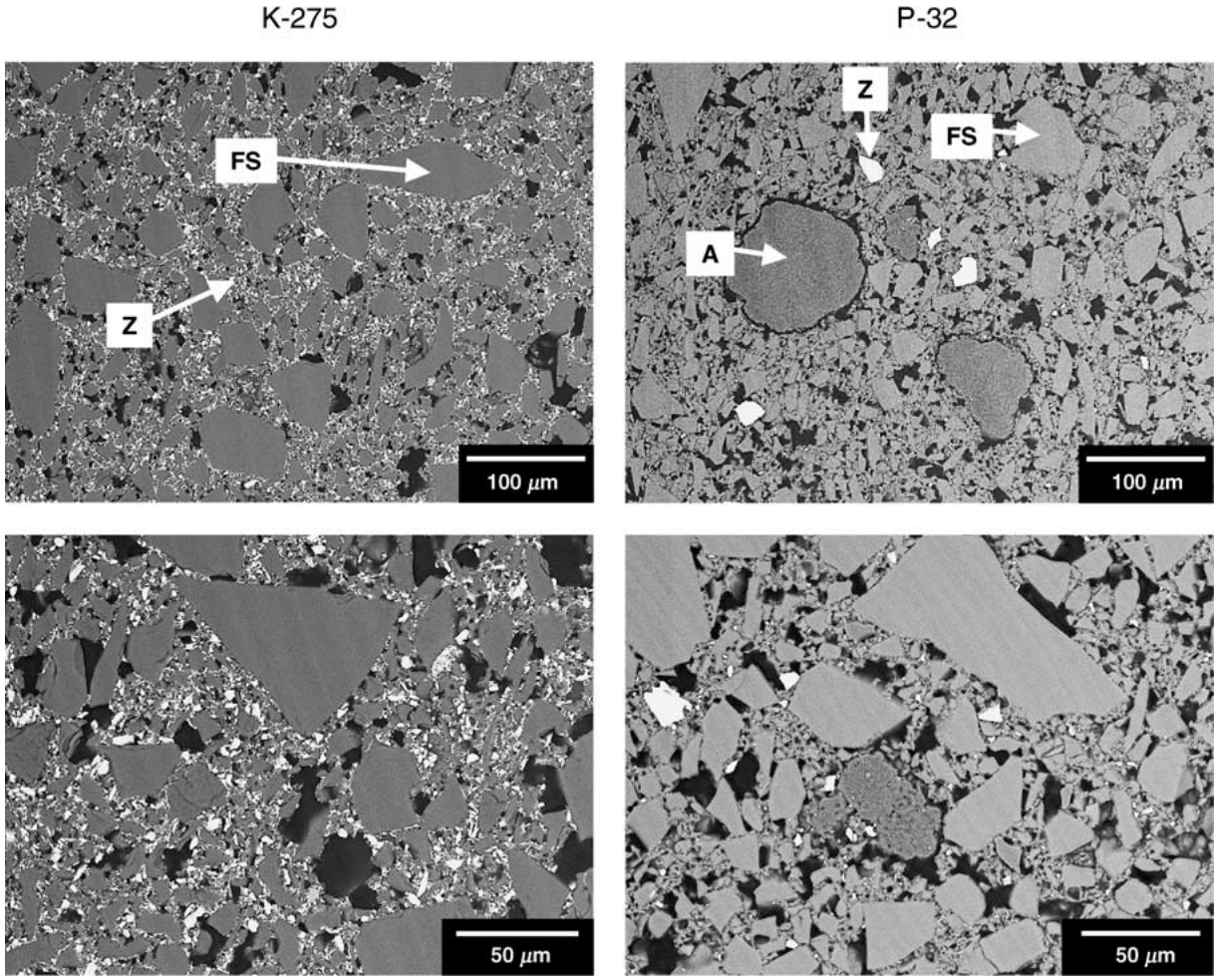

Figure 2 Microstructures of the two as-received ceramic cores at different magnifications. (SEM-BSE). A = alumina, FS = fused silica, and Z = zircon.

have small or thin cross-sections that are more compatible to a silica/zircon composition, and the other was a high silica ceramic used in the manufacturing of directionally-solidified or single crystal superalloy components where complete chemical leachability is crucial. The differences in zircon content between the two ceramics were an order of magnitude and this served as a suitable independent parameter in this study.

2. Experimental descriptions

2.1. Materials and specimen geometry

The examined silica/zircon ceramic, designated as K-275, had a primary chemistry of 74 wt% silica (SiO_2) and 24 wt% zircon ($ZrSiO_4$) and 1% alumina (Al_2O_3) and the high silica ceramic, designated as P-32, had a primary chemistry of 93 wt% SiO_2, 3 wt% $ZrSiO_4$, and 4% Al_2O_3. Both ceramic compositions are categorized as "Type-B" silicas in refractories terminology according to ASTM C416 (i.e., the sum of the alumina and twice the alkali oxides contents exceed 1.5%) [7].

Microstructures of both ceramics are shown in Fig. 2, and manufacturer's reported data for each are listed in Table I. The grain size distributions in Fig. 2 are qualitatively consistent with information presented in Table I. The maximum grain size in Table I only pertains to the upper limit of each core's grain size distribution; it does not fully portray information about the whole size distribution like Fig. 2 illustrates. The smaller fused silica grains in the P-32 are consistent with its higher reported surface area of initial fused silica grains that were used to batch it. The K275 ceramic is characterized by extremely high content of zircon in the matrix, and contains predominantly fused silica grains (some cristobalite is also observed) in a fine and porous silica and zircon matrix. Zircon is again mainly present as (uniformly distributed) fine-grained zircon flour but some larger grains were also observed. The P32 ceramic predominantly contained fused silica, some cristobalite, alumina agglomerate, and small amounts of zircon, with the latter present mainly as fine-grained zircon (1–10 μm). The microstructure is characterized by a very porous and fine matrix, in which fine-grained zircon is dispersed. Agglomerated alumina grains are almost totally separated from surrounding grains. The P-32 ceramic tended to have an overall finer average grain size than the K-275 ceramic. Additional differences between the ceramics may be compared in Table I (e.g., the silica/zircon ceramic had a lower initial cristobalite content, lower initial bulk porosity, and higher initial bulk density than the high silica ceramic).

Cylindrical test specimens were prepared from both ceramics. Green-state injection molding was used to form the cylinders, and then both materials were sintered under the same sintering schedule.[§] The final nominal dimensions of each cylindrical specimen used

[§] The sintering temperature and profile are proprietary; however, it may be stated that the sintering temperature was less than the lowest isothermal temperature (1475°C) investigated in this study.

TABLE I Manufacturers reported data for the tested ceramics

Material ID	Major chemistry	Content (wt%)	Maximum grain size (μm)	Surface area of initial fused silica ($m^2\ g^{-1}$)	Initial cristobalite content (%)	Cristobalite content after 30 min at 1530°C (%)	Mineralizer	Initial bulk porosity (%)	Initial bulk density (g/cc)
K-275	SiO_2	74							
	$ZrSiO_4$	24	74	1.46	8	35	MgO	28.0	1.83
	Al_2O_3	1							
P-32	SiO_2	93							
	$ZrSiO_4$	3	74	2.65	13	57	MgO	30.0	1.60
	Al_2O_3	4							

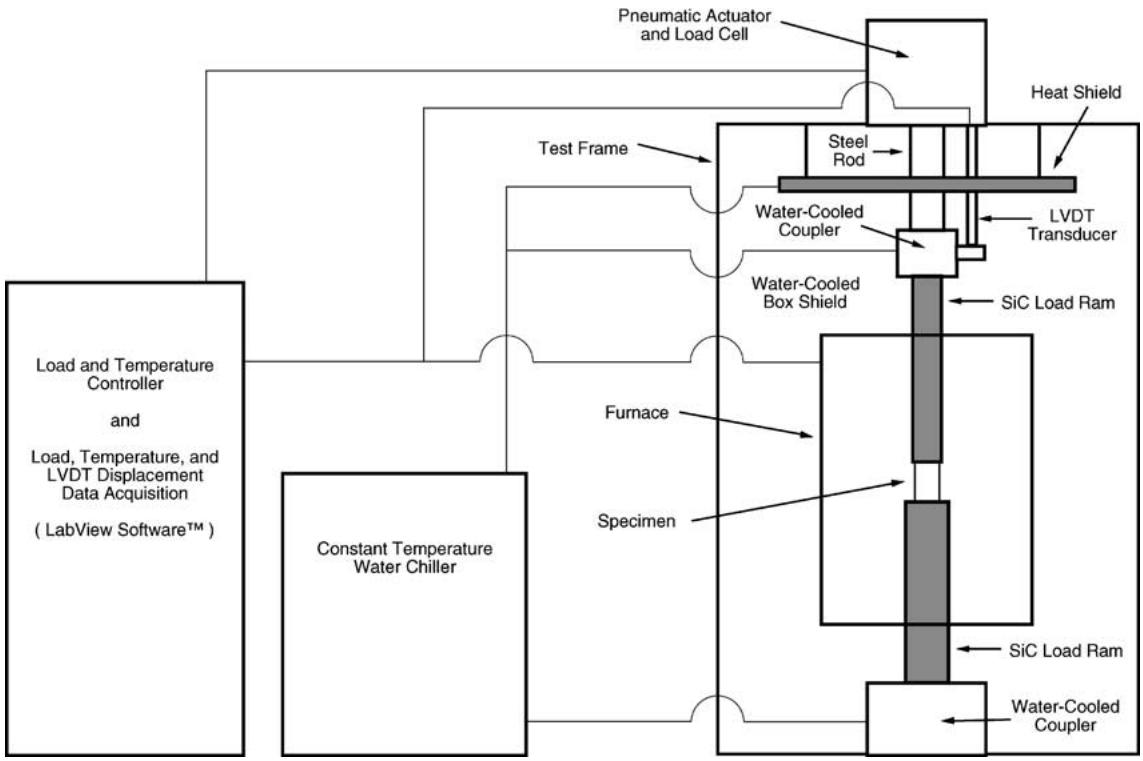

Figure 3 Schematic of the creep test apparatus. Apparent dilation during specimen heating was also measured with this unit.

for testing were a 9.2 mm diameter and a 25.4 mm length. Using an appropriate aspect ratio (L/D) for compression testing is an important consideration for valid testing. A L/D of 2.6 or greater is recommended for *compressive strength tests* so that the friction effects between the specimen ends and loading ram are small compared to the axially applied compressive stresses [8]. In the present study, the L/D was approximately 2.8 so stresses and strains due to such friction were believed to be negligible. Lastly, only specimens whose ends were parallel and that were perpendicular with the length (tolerances for both within 0.02 mm) were used for testing to avoid the introduction of unacceptably high bending strains and the misleading results that they can cause.

2.2. Test facility and procedure

A schematic of the test apparatus used is shown in Fig. 3. The test frame consisted of a digitally controlled (LabVIEW^{TM} software, National Instruments, Austin, TX) pneumatic actuator that transferred load to the test specimen through sintered α-SiC (Hexoloy SA^{TM}, Carborundum Co., Niagara Falls, NY) push rods. The push rods were concentrically aligned through translatable adjustments in the load-train's bottom mount, while axial alignment was accomplished through adjustments about a spherical bearing (also in the bottom mount). The load-train was surrounded by a resistance-heated clamshell furnace (Model 3320, Applied Test Systems, Inc., Butler, PA) that was capable of heating to at least 1525°C in ambient air. Within ASTM guidelines [9], temperature fluctuations were approximately ±2°C and load fluctuations were less than 1% of mean test load. The grips (that connected the push rods to the test frame or its load cell/actuator) were water-cooled using a closed-system water-circulating reservoir. Lastly, a linear variable differential transducer (LVDT) was used to continuously measure the specimen's axial dimensional change due to heating and the applied compressive load (after the subtraction of load-train dilatational effects).

All testing was conducted using the thermomechanical profile illustrated in Fig. 4, which is an example of an investment casting profile. After each cylindrical specimen was inserted into the test frame, they were held under a constant low-valued compressive stress (approximately 0.2 MPa = 29 psi) during heating. This pre-load served to keep the load train and specimen

TABLE II Description of thermomechanical test profile matrix

Thermo-mechanical profile ID	Heat up condition	Soak/creep condition	Cool down condition
1	300°C/h to 1475°C at 0 MPa (aging)	1 h at 1475°C at 0 MPa (aging)	900°C/h to 1150°C at 0 MPa (aging)
2	300°C/h to 1475°C at −0.17 MPa	1 h at 1475°C at −2.07 MPa	900°C/h to 1150°C −2.07 MPa
3	300°C/h to 1475°C at −0.17 MPa	1 h at 1475°C at −4.14 MPa	900°C/h to 1150°C at −4.14 MPa
4	300°C/h to 1475°C at −0.17 MPa	1 h at 1475°C at −6.21 MPa	900°C/h to 1150°C at −6.21 MPa
5	300°C/h to 1525°C at 0 MPa (aging)	1 h at 1525°C at 0 MPa (aging)	900°C/h to 1150°C at 0 MPa (aging)
6	300°C/h to 1525°C at −0.17 MPa	1 h at 1525°C at −2.07 MPa	900°C/h to 1150°C at −2.07 MPa
7	300°C/h to 1525°C at −0.17 MPa	1 h at 1525°C at −4.14 MPa	900°C/h to 1150°C at −4.14 MPa
8	300°C/h to 1525°C at −0.17 MPa	1 h at 1525°C at −6.21 MPa	900°C/h to 1150°C at −6.21 MPa

Conversions: 2.07 MPa = 300 psi, 4.14 MPa = 600 psi, and 6.21 MPa = 900 psi, 300°C/h = 540°F/h and 900°C/h = 1620°F/h, 1475°C = 2685°F and 1525°C = 2775°F.

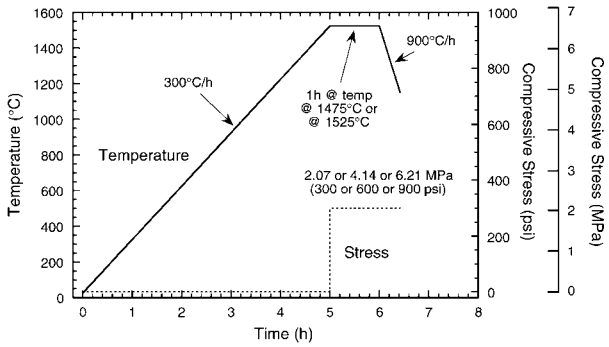

Figure 4 Schematic of the test temperature- and stress-histories used in the tests.

sufficiently seated, as well as permitted the continuous measurement of specimen length during heating.[¶] All specimens were heated at a rate of 300°C/h to either 1475 or 1525°C. Because the high-temperature furnace was difficult to tune below approximately 450°C (it had a type B control thermocouple), only dilatational measurements above that were considered valid. Once 1475 or 1525°C was attained, a compressive stress of 2.07, 4.14, or 6.21 MPa (300, 600, or 900 psi, respectively) was then applied. A compressive stress imposition of approximately 4 MPa onto the ceramic is not uncommon in service, so the stress range of ∼2–6 MPa was chosen to bracket that value. The loaded specimen was then held at constant temperature and stress for 1 hour. The specimen was then cooled at a rate of 900°C/h (under stress) to ambient temperature. The specimen length was continuously measured using the test frame's LVDT during the thermomechanical profile, and digitally acquired with the computer.

The investigated test matrix is outlined in Table II, and specimens from both ceramics were evaluated (16 total or 8 specimens from each ceramic). To examine what effect the sole thermal profile had on dimensional changes, as-received specimens from both ceramics were exposed to just temperature (i.e., no stress), and they are referred to hereafter as "aged" specimen tests.

[¶] Interrupted tests were performed with both ceramic cores to examine if this 0.2 MPa pre-load was imparting compressive creep into the specimens during heating to 1525°C (the higher of the two test temperatures, and potentially worst-case scenario). The length of pre-loaded specimens was compared to "aged" (no stress) specimens that were subjected to the same thermal schedule. The apparent length changes for both pre-loaded and "aged" specimens were equivalent; thusly, it was concluded that the pre-loading did not significantly alter the material's response during heating.

2.3. Dimensional changes and creep analyses

Dimensional changes of specimens from both ceramics were examined in two ways: through the comparison of apparent thermal expansion behavior during heating and before-and-after geometrical changes (i.e., changes in length and diameter).[**] The continuous LVDT measurements were used to compare the apparent thermal expansion behavior. This was accomplished by first subtracting out the thermal expansion of the whole load-train from the raw LVDT data from each test, with the former measured from a test with an α-SiC cylindrical specimen having the same nominal length (and a known thermal expansion coefficient) as the ceramic core specimens. A micrometer was used to measure the before-and-after geometrical changes in both ceramics, and the results were used to compare the dimensional changes that were a consequence of the whole thermomechanical profile.

Compressive creep deformation analysis was enabled using the continuous LVDT data during the one-hour hold segment. Apparent machine compliance was first measured at both temperatures and all three stresses using the same α-SiC cylindrical specimen geometry described in the preceding paragraph, and then subtracted from the LVDT raw data from each test. Compressive creep strain was then analyzed as a function of time, stress, and temperature.

Classical creep analysis often involves the determination of a steady-state creep rate as a function of applied stress and temperature, and the examination of this relationship was pursued in the present study for the one-hour-long isothermal/isostress segment. The steady-state compressive creep rate ($d\varepsilon/dt_{ss}$) is typically related to the applied compressive stress and temperature using an empirical Arrhenius power-law formulation or the familiar Norton-Bailey creep equation [10]:

$$d\varepsilon/dt_{ss} = A\sigma^n \exp(-Q/RT), \qquad (1)$$

where A is a constant, σ is the applied stress, n is the creep-rate stress exponent, Q is the activation energy,

[**] Due to the rapid cooling rate (900°C/h) and the consequential rapid load train dimensional contractions (and the relatively high uncertainty in instantaneous specimen length during this part of the thermal profile), dimensional change comparisons during the cooling segment were not compared. However, their effects are inherently part of the before-and-after dimensional changes.

R is the gas constant, and T is the absolute temperature. Multi-linear regression of the log-log form of Equation 1 is then performed to determine the constants A, n, and Q for each material. By performing the analysis in this manner, it is implicitly assumed that the same dominant (or rate-limiting) creep mechanism is active at all temperatures and stresses for a given material. Furthermore, the material whose creep is analyzed after Equation 1 is generally assumed to initially be fully dense. The validity of this assumption is assessed through the goodness-of-fit of this regressed equation to the experimental data, the reasonableness of the obtained values for n and Q, and whether or not the existence of material state equilibrium can be subsequently proven for all temperatures and stresses.

2.4. High temperature X-ray diffraction analyses

In situ high temperature x-ray diffraction was used to investigate cristobalite phase precipitation as a function of time and temperature. Data was collected using an automated X-ray powder diffractometer [Model PADX, Scintag Inc., Cupertino, CA] with a Cu normal focus X-ray tube operated at 45 kV and 20 mA and an mBraun linear position sensitive detector (PSD). A Buehler HDK 2.3 high temperature X-ray furnace attachment was operated with a platinum-30% rhodium resistance strip heater. Powder samples were dispersed on the top surface of the heater strip and studied in stagnant air. The system is described in detail in [11].

A thermocouple (Type S) was spot-welded to the bottom of the heater strip to measure and control the temperature to a precision of 0.5°C. Accuracy of the temperature is less simple to define since the surface of such samples is often cooler than the bulk and the point where the temperature was measured was not the same as the location of the diffracting volume [12]. The temperature was stepped from 1000°C to 1530°C with 30 seconds for data collection at 10°C temperature increments using the PSD in stationary mode, in which a 2θ range from 19° to 29° was collected without moving the detector. This angular range allowed us to monitor the increase in intensity of the main cristobalite diffraction peak, indicating increased % crystallinity, as the temperature was increased.

3. Results and discussion

A comparison of the performances of the silica/zircon and high silica ceramic is made with respect to various segments in the profile illustrated in Fig. 4. Firstly, the differences in apparent dilatation behavior during the heating segment are examined. The creep responses during the one-hour isostress segment are then interpreted. Lastly, the dimensional changes that resulted from the entire thermomechanical profile are examined.

3.1. Dimensional changes during heating

Both ceramics exhibited: a relatively low, constant, apparent coefficient of thermal expansion (AppCTE) between 500 and 1100°C; a minima in the AppCTE at approximately 1300°C, and; a relatively high AppCTE between 1350°C and 1525°C. These effects are illustrated in Fig. 5.

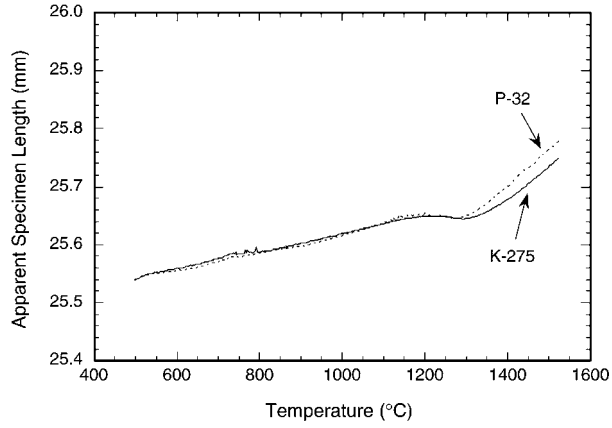

Figure 5 Specimen elongation curves during heatup to 1525°C for the K-275 and P-32 core ceramics.

Note that "apparent" specimen lengths are reported. The shown length measurements in Fig. 5 are inferred from the LVDT measurement after load-train thermal expansion was subtracted out (i.e., reporting a quantified instantaneous length is probably not accurate, such as it would be with a dual-rod dilatometer for example). Additionally, because the length is "apparent", the authors hesitate to report a coefficient of thermal expansion for the 500–1100°C temperature range.

The decrease in the AppCTE between 1100 and 1300°C is probably associated viscous flow sintering [3] with the initiation of cristobalite formation around 1300°C contributing to its decrease {and the fact that the density of cristobalite (2.32 g/cc) is greater than that of fused silica (2.23 g/cc)}. High temperature x-ray diffraction data were collected on the high silica ceramic to examine this further. The primary cristobalite peak as a function of temperature is shown in Fig. 6 and confirms the onset of increased cristobalite concentration (i.e., an increase in its relative intensity) at approximately 1300°C. The rate of crystallization of fused silica to cristobalite can depend on several parameters (e.g., type of impurity, impurity content, cristobalite seed content, etc.) and its temperature of activation can be altered somewhat; however, the literature suggests its initiation from fused silica occurs at or near 1300°C [3, 6, 13] which is consistent with what is shown in Fig. 6.

The specimen length-temperature curves for these materials diverged at approximately 1300°C with the length of the K-275 silica/zircon ceramic increasing at a slower rate than the P-32 high silica ceramic above that temperature (see Fig. 5). This slower rate of dilation in the K-275 compared to that of the P-32 is consistent with: observations in the literature [6] that zircon enhances the crystallization of fused silica (K-275 has an order of magnitude higher concentration of zircon than P-32 has; and the fact that the fused silica powder in the P-32 had a small grain size (i.e., greater surface area) than the K-275. As crystallization of the fused silica occurs during heating to either of the examined isothermal temperatures, cristobalite heterogeneously nucleates at the surfaces of individual fused silica particles and a crystalline front advances radially inward

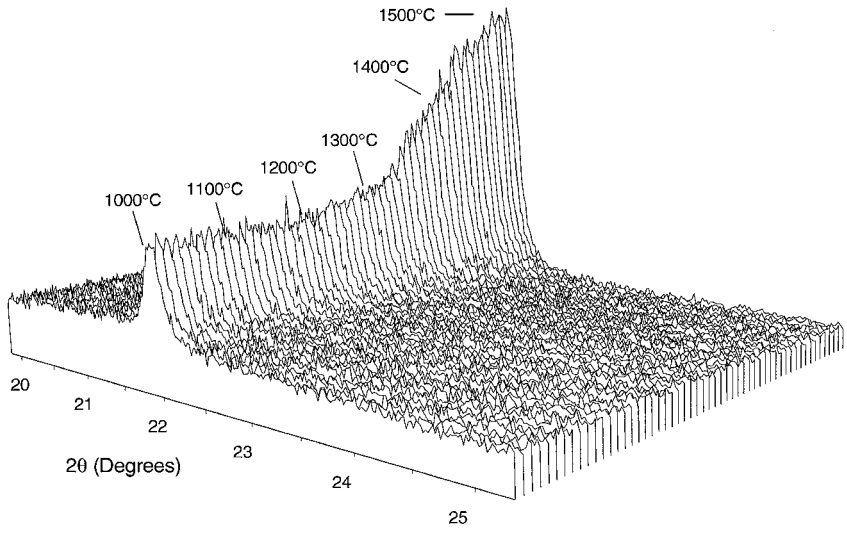

Figure 6 Cristobalite content increased during heating as evidenced by increasing peak intensity obtained from high temperature x-ray diffraction. Data for P-32 core ceramics shown.

at the expense of the amorphous interior. Fused silica particles having a larger surface-area-to-volume ratio (i.e., those that were in P-32) fully crystallize more quickly [14]. This crystalline "shell" inhibits further viscous flow of that particular fused silica grain and shrinkage ceases. The observed dimensional changes are therefore a result of a time- and temperature-dependent competition between the two thermally activated processes of viscous flow of the fused silica and nucleation and growth of the consuming cristobalite. Greater concentrations of zircon expedite cristobalite formation so less shrinkage would be expected than if lesser concentrations were present. This is consistent with differences in elongation occurring in Fig. 5.

3.2. Creep deformation

The silica/zircon and high silica ceramics had different creep resistances during the one-hour isothermal/isostress segment of the profile illustrated in Fig. 4. Apparent creep strain as a function of time for the different test temperatures and stresses are shown in Fig. 7a–b. The silica/zircon ceramic crept more than the high silica ceramic at the same stress/temperature/time condition, and this is summarized in Table III. The creep curves generally exhibited primary creep during the first 30 minutes and a steady-state (i.e., constant creep rate) creep response thereafter. The last 10–15 minutes of the creep strain-time curve for each test was linearly

TABLE III Total accumulated compressive creep strain during 1 h hold at temperature

ID	K-275	P-32
1	N/A	N/A
2	−0.135%	−0.097%
3	−0.367%	−0.186%
	−0.359%	−0.170%
4	−0.585%	−0.257%
5	N/A	N/A
6	−0.219%	−0.150%
7	−0.564%	−0.361%
	−0.581%	−0.310%
8	−1.008%	−0.456%

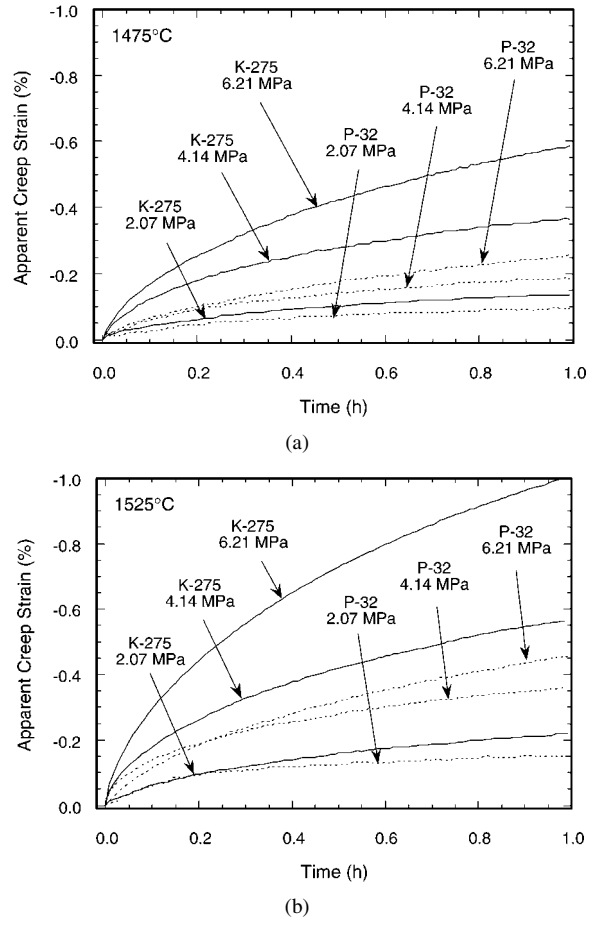

Figure 7 Creep strain histories of the two silica core ceramics during their one-hour isothermal and isostress segment at (a) 1475°C and 2.07, 4.14, and 6.21 MPa, and (b) 1525°C and 2.07, 4.14, and 6.21 MPa.

regressed to calculate an apparent steady-state creep rate (see Table IV); those rates were used in the analysis whose description follows.

The apparent steady-state creep-rates for all tests for both ceramics were multilinearly regressed against stress and temperature using Equation 1. The values for the constants in that equation are summarized in Table V, and the resulting regressed lines are shown in Fig. 8. The K-275 ceramic crept at a faster rate

TABLE IV Summary of steady-state creep rates

ID	K-275	P-32
1	N/A	N/A
2	−0.070%/h	−0.038%/h
	−0.195%/h	−0.118%/h
3	−0.223%/h	−0.118%/h
4	−0.363%/h	−0.140%/h
5	N/A	N/A
6	−0.112%/h	−0.062%/h
	−0.224%/h	−0.145%/h
7	−0.262%/h	−0.159%/h
8	−0.466%/h	−0.253%/h

TABLE V Parameters describing the minimum creep rate dependence on stress and temperature

Parameter	K-275	P-32
A, Pre-exponential constant (h^{-1} MPa^{-n})	2.83×10^2	3.01×10^4
n, Stress exponent (±95% conf. est.)	1.4 (1.1, 1.6)	1.3 (0.9, 1.6)
Q, (kJ mol^{-1}), Activation energy (±95% conf. est.)	130 (30, 240)	210 (70, 340)
Number of specimens	8	8
R^2, Statistical residual of multilinear regression	0.98	0.96

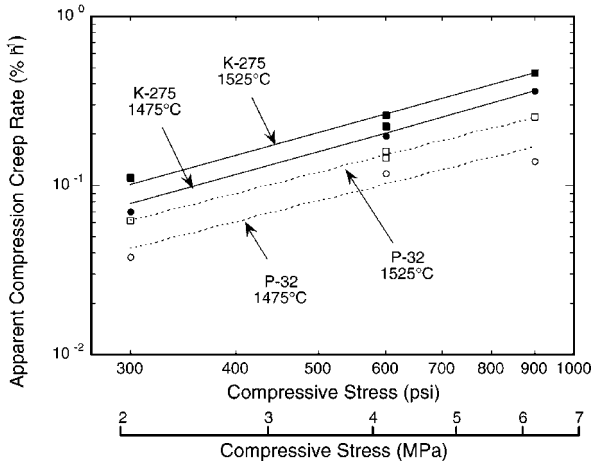

Figure 8 Compression creep rate as a function of stress and temperature for the K-275 and P-32 core ceramics. Creep rate was calculated using linear regression of the creep strain - time curve over the last ten minutes of the one-hour segment.

than the P-32 ceramic for any given stress/temperature combination. As mentioned previously, the regression against Equation 1 assumes that the same rate-limiting mechanism is controlling steady-state creep at all temperatures and stresses and that the material state is in equilibrium; though unproven, the latter may not be a valid assumption owing to the changing level of cristobalite content that may be occurring during the isothermal/isostress creep segment.†

The creep-rate stress exponent, n, is equivalent (within 95% confidence) in value (1.3–1.4) for the two ceramics, and they are illustrated in Fig. 8 by the slopes of the fitted lines. This suggests (statistically) that the differences in zircon concentration (3 vs. 24%) in these two ceramics did not affect the apparent steady-state creep-rate's dependence on stress. An exponent equaling unity would be expected if diffusion were the rate-limiting mechanism [15]; however, owing to the large amount of porosity in the both as-received ceramics (28–30%), some power-law creep/sintering effect is likely occurring [16–18] and contributing to the apparent creep rate dependence on applied stress with the result that $n > 1$. Additionally, if any of the grains are not fully crystalline, and if they fracture as consequence of any high-stress-concentration grain-to-grain mechanical loading, then greater amounts of cristobalite formation would be expected owing to the greater amount of fused silica surface area that would be created.

The activation energy for the apparent creep deformation for both ceramics was statistically equivalent (130 and 210 kJ/mol—average of 170 kJ/mol) within 95% confidence. This suggests that the differences in zircon concentration in these two ceramics did not affect the apparent steady-state creep-rate's dependence on temperature. Their values are qualitatively illustrated in Fig. 8 by the spread in the pair of fitted lines for either ceramic. Almost all the literature that involve the study of cristobalite crystallization, viscous flow, and sintering activation energies report higher-values (≈400–700 kJ/mol) than what was determined in the present study; however, they generally were studies that involved either relatively low temperatures or wide temperature ranges or both (900 to 1500°C) [4–6, 19, 20]. An exception to this trend is the work of Takayangi and Katashima [21] whose activation energy analysis was an outcome of a higher, and relatively narrow, test temperature range of 1500 and 1680°C. Takayangi and Katashima reported crystallization activation energies of 180 and 213 kJ/mol that are equivalent to the values determined in the present study. From this, it is concluded that the continued crystallization of cristobalite during the isothermal/isostress segment dominates the apparent steady-state creep-rate dependence on temperature between 1475 and 1525°C.

It is noted that the utilization of a conventionally used power-law creep model in this study proceeded with caution. Material state equilibrium is implicitly assumed in its use and the authors have reason to believe that a state of nonequilibrium existed (i.e., changing cristobalite content) during the isothermal/isostress segment.

3.3. Whole thermomechanical profile effect on dimensional changes

The microstructures of both ceramics changed as a consequence of the used thermomechanical profile. A comparison of Figs 2 and 9 show that much of the fused silica had converted to cristobalite (as evidenced by "fish-scale" granular structure that is characteristic of cristobalite) and that its original average grain size had reduced. The zircon grains were relatively unchanged in size as a consequence of the test profile. The radially advancement of cristobalite can be seen on some of the grains in the microstructures shown in Fig. 9, especially in the P-32 ceramic. The before-and-after microstructures of the K275 ceramic were quite similar

† Experimental difficulties associated with the heating of the sample in the hot x-ray diffractometer did not allow the authors to examine cristobalite content during the isothermal hold segment.

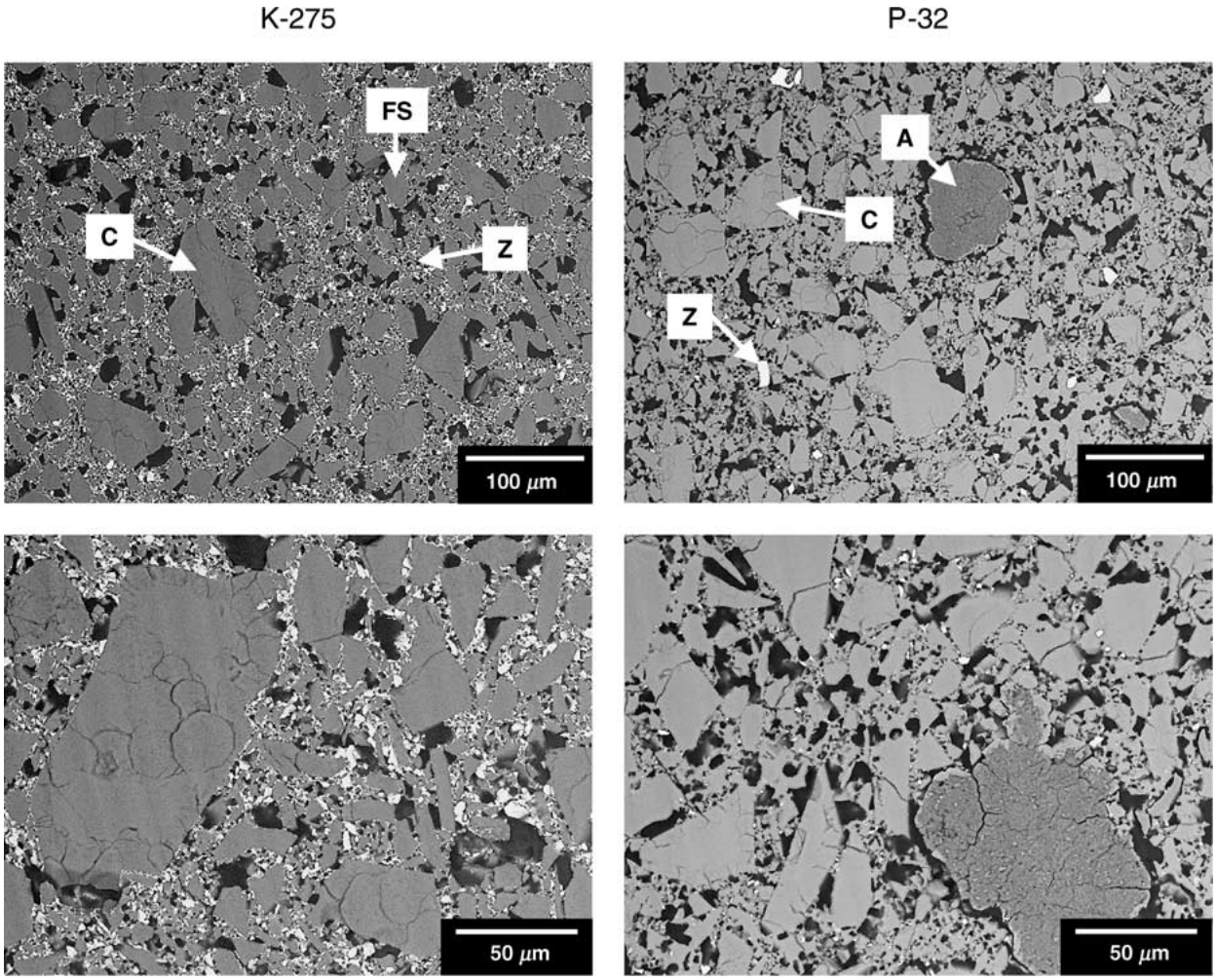

Figure 9 Microstructures (at different magnifications) of the two ceramic cores after they were tested at the condition that included the 1525°C and 6.21 MPa creep segment. (SEM-BSE). A = alumina, C = cristobalite, FS = fused silica, and Z = zircon.

but the latter had a higher cristobalite content. Weaker bonding among the grains appeared to exist in the microstructures that suggest that the zircon may have hampered sintering of the fused silica (its contribution to the conversion of fused silica to cristobalite cannot be discounted though). The strong bond formation in the matrix is very clearly observed in the P32 ceramic. The porosity appears to have increased as well.

The total contraction for both the silica/zircon and high silica core pairs tended to be dominated by sintering and cristobalite formation that occurred during the heating segment of the thermomechanical profile. The silica/zircon cores generally exhibited less total contraction than the high silica cores for a specific test condition; this is consistent with there being both less initial surface area of fused silica grains and a higher concentration of zircon as discussed in Section 3.1. Examination of Fig. 10 shows that approximately 1% (±0.2%) axial contraction had occurred in the absence of stress; a typical amount observed in service. The application of a compressive stress onto the K-275 specimens did not appreciably contract them further unless they were loaded at 6.21 MPa at 1525°C (where the contraction had doubled over that of the unstressed condition). The application of a compressive stress onto the P-32 specimens further contracted them another 75% over that of the unstressed condition; however, that contraction

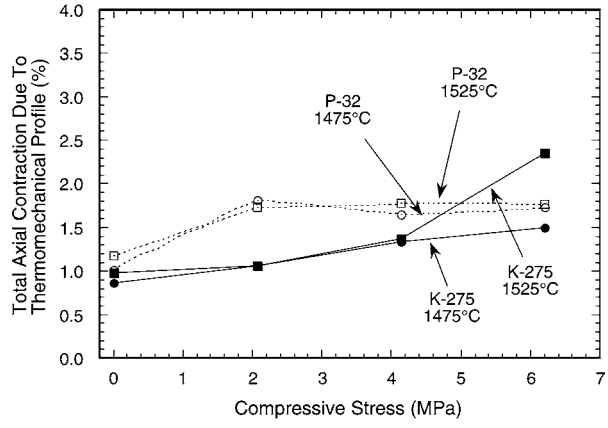

Figure 10 Total axial change in length due to thermomechanical profile for the comparison of the K-275 and P-32 core ceramics.

appeared to be independent of the applied stress level. Those added contractions due to the application of compressive stress are too amounts typically observed in service.

Further evidence that most of the contraction (or densification) in both ceramic had occurred during heat up is shown in Fig. 11a and b. As expected from the results portrayed in Fig. 10, the bulk densities of both ceramics had increased (same mass and contracted dimensions) as a consequence of testing. Exposing both ceramics

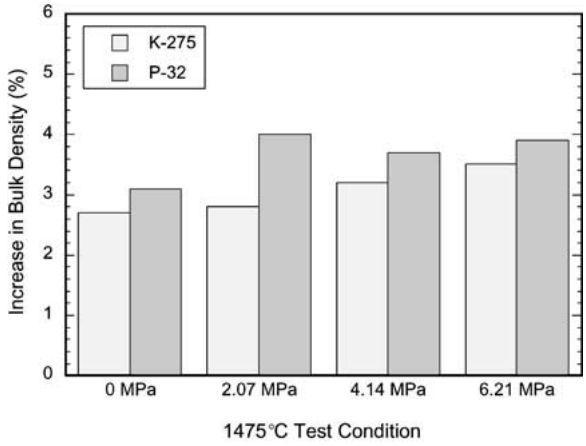

(a)

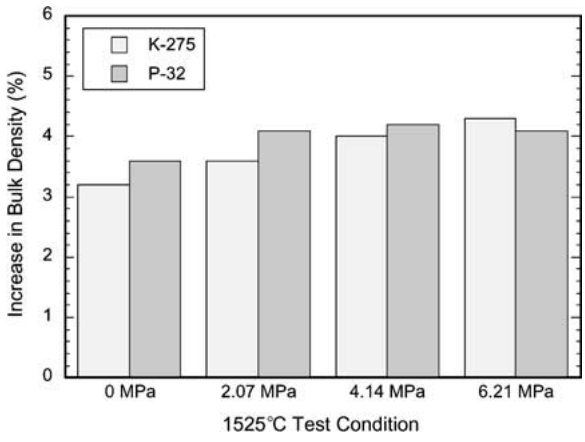

(b)

Figure 11 Bulk density increase of the two silica core ceramics subjected to 0, 2.07, 4.14, and 6.27 MPa during the one-hour isothermal segment at (a) 1475°C and (b) 1525°C.

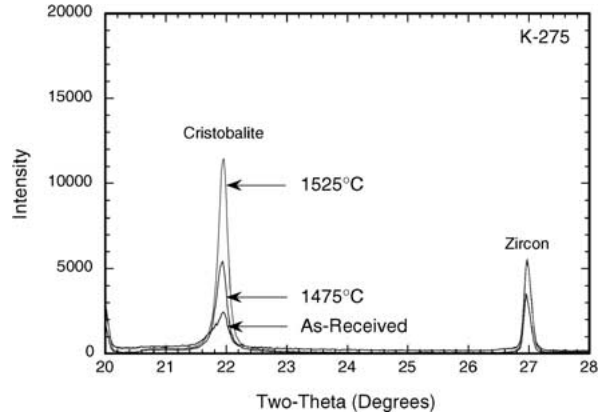

(a)

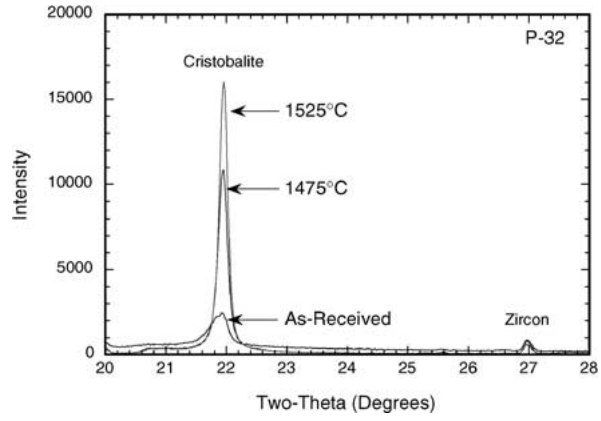

(b)

Figure 12 X-ray diffraction spectra of the (a) K-275 and (b) P-32 core ceramics after thermal cycling showing cristobalite's [101] peak at $2\theta = 21.91^\circ$ and zircon's [200] peak at $2\theta = 26.96^\circ$. As-received spectra are compared to those from one-hour isothermal segments at 1475 and 1525°C.

to solely the thermal profile (no stress) resulted in bulk density increases on the order of 3–3.2%. Although the axial contractions outlined in Fig. 10 acted to further densify the ceramics, their contributions to the total densification were somewhat minor (however, their creep-rate (or densification-rate) during the isostress segment were found to have power-law dependencies as discussed in Section 3.2). There tended to be greater densification for the P-32 ceramic than the K-275 ceramic; this shows that the levels of initial fused silica content in these two ceramics had more of an impact on the amount of densification than the initial cristobalite and porosity contents had (see Table I).

The degree of cristobalite formation and the measured bulk densities that had changed as a consequence of the thermal (no stress) profile show that the porosity content in both ceramics had increased. Besides the high temperature X-ray diffraction (XRD), room temperature XRD was used to quantify the cristobalite content in the as-received, 1475-, and 1525°C-aged states (at room temperature after their thermal cycling) of both ceramics, and their results are summarized in Table VI. A qualitative examination of the thermal profile effect on cristobalite may be made using in Fig. 12a and b. Samples from each condition were ground with a mortar and pestle and equal volumes of each were

TABLE VI Comparison of predicted and measured contraction due to crystallization of fused silica to cristobalite

Material	Condition	Wt% cristobalite	% Total silica that is cristobalite	Measured% densification (no stress)	New porosity content (%)
K-275	Pure fused silica	0	0		
	As-received	7.4	10	0.00	28.0
	1475°C	37.2	50	0.87	28.3
	1525°C	42.5	57	1.06	28.4
	Pure cristobalite	100	100		
P-32	Pure fused silica	0	0		
	As-received	7.5	8	0	30.0
	1475°C	57.6	62	1.02	30.7
	1525°C	68.8	74	1.18	30.9
	Pure cristobalite	100	100		

Densities: fused silica = 2.23 g/cc; cristobalite = 2.32 g/cc.

sampled, and compared against a cristobalite standard. The shown cristobalite peak intensity is then proportional to its weight fraction in each ceramic. One may calculate the change in porosity based on the combination of the quantified cristobalite results with densities of 2.23 g/cc for fused silica and 2.32 g/cc for cristobalite, 4.56 g/cc for zircon, and 3.98 g/cc for alumina. When this is done, it is found that the initial porosity content of 28.0% in the K-275 ceramic had increased to 28.3 and 28.4% when the isothermal segment was at 1475 and 1525°C, respectively. Likewise, the initial porosity content of 30.0% in the P-32 ceramic had increased to 30.7 and 30.9% as a consequence of exposure to those two isothermal profiles. The porosity content in the P-32 ceramic had increased more than in the K-275 ceramic owing to its greater amount of initial fused silica. As shown in Figs 10 and 11, the application of stress densified these ceramics further (with a power-law rate dependence) presumably through the slight lessening of this porosity level; however, that contribution to the total densification was not as significant as the densification from just each ceramic's exposure to the employed temperature profile.

The dimensional changes and creep results of the ceramics evaluated in the present study may be used to improve the casting process involving them because their results enable better and more confident predictability and control of crushability and stability of cores made from them. Thermomechanical conditions during casting may be altered so that either investigated ceramic core creeps rapidly enough to avoid defect creation in the metal components while being sufficient creep resistant to maintain dimensional tolerances.

4. Conclusions

Dimensional changes and creep deformation were characterized in a 74% silica, 24% zircon and a 93% silica, 3% zircon ceramic and compared. All specimens were tested with a thermal profile that consisted of a 300°C/h heating rate to 1475 or 1525°C, followed by a one-hour isothermal hold (where each specimen was compressively crept under a static stress of 2.07, 4.14, or 6.21 MPa), and followed by a 900°C/h cooling rate under that same stress. Reinitiated sintering and subsequent cristobalite formation that occurred during the heating segment dominated the total contraction for both ceramics. The silica/zircon ceramic generally exhibited less total contraction than the high silica ceramic for a specific test condition.

Compressive creep strains did add to the total measured contraction in both ceramics; however, their contribution was minor. Creep-rate stress exponents and activation energies were equivalent (within 95% confidence) for both materials suggesting that the different content of zircon did not affect creep-rate dependence on stress and temperature. The $n \approx 1.3$–1.4 indicated that diffusion-assisted crystallization of cristobalite, combined with power-law sintering (owing to the high levels of initial porosity), and was likely the rate-limiting mechanism in the apparent creep deformation for both ceramics.

Lastly, due to the non-equilibrium state exhibited by both ceramics during the investigated thermal profile, the utilization of a conventionally-used power-law creep model should proceed with caution because the existence of material state equilibrium is implicitly assumed in its application.

Acknowledgments

Research sponsored by the U. S. Department of Energy, Assistant Secretary for Energy Efficiency and Renewable Energy, Office of Transportation Technologies, as part of the High Temperature Materials Laboratory User Program under Contract DE-AC05-00OR22725, managed by UT-Battelle, LLC. The authors wish to thank E. S. Chin and J. J. Swab for reviewing the manuscript and for their helpful comments.

References

1. E. SACHS, M. CIMA and J. BREDT, in "Intelligent Design and Manufacturing for Prototyping," ASME PED-Vol. 50 (1991) p. 61.
2. S. URAM, *Foundry* July (1971) 48.
3. I. C. HUSEBY, M. P. BOROM and C. D. GRESKOVICH, *Ceramic Bulletin* **58** (1979) 448.
4. V. ZANDIAN, J. S. FLORRY and D. TAYLOR, *British Ceramic Transactions* **92** (1993) 155.
5. L.-Y. WANG and M.-H. HON, *Journal of the Ceramic Society of Japan* **102** (1994) 517.
6. *Idem*., *Ceramics International* **21** (1995) 187.
7. "Standard Classification of Silica Refractory Brick," ASTM C416, Vol. 15.01 (American Society for Testing and Materials, West Conshohocken, PA, 1998).
8. S. SHIN and O. BUYUKOZTURK, US DOE Report ORNL/Sub/79-07862/02 (1990).
9. "Standard Test Method of Measuring the Thermal Expansion and Creep of Refractories Under Load," ASTM C832, Vol. 15.01 (American Society for Testing and Materials, West Conshohocken, PA, 1998).
10. F. H. NORTON, "The Creep of Steel at High Temperature" (McGraw-Hill, New York, 1929).
11. E. A. PAYZANT and W. S. HARRISON III, *Advanced X-Ray Analysis* **43** (2000) 267.
12. H. WANG and E. A. PAYZANT, in Thermosense XXI—Proceedings of SPIE, Vol. 3700, (1999) p. 377.
13. K. KATO and Y. NOZAKI, *Imono* **62** (1990) 726.
14. I. B. CUTLER and R. E. HENRICHSEN, *J. Amer. Ceram. Soc.* **51** (1968) 604.
15. W. R. CANNON and T. G. LANGDON, *J. Mater. Sci.* **18** (1983) p. 1.
16. H. PALMOUR III and D. R. JOHNSON, in "Sintering and Related Phenomena," edited by G. C. Kuczski *et al*. (Gordon and Breach, New York, 1967) p. 779.
17. D. S. WILKINSON and M. F. ASHBY, *Acta Metallurgica* **23** (1975) 1277.
18. *Idem*., *Science of Sintering* **10** (1978) 67.
19. G. HETHERINGTON, J. H. JACK and J. C. KENNEDY, *Physics and Chemistry of Glasses* **5** (1964) 130.
20. F. E. WAGSTAFF, *J. Amer. Ceram. Soc.* **52** (1969) 650.
21. T. TAKAYANAGI and S. KATASHIMA, *Imono* **60** (1988) 401.

Received 1 March 2001
and accepted 25 April 2002